LAWRENCE
LIVERMORE
NATIONAL
LABORATORY

UCRL-TH-217754

Ion Deflection for Final Optics in Laser Inertial Fusion Power Plants

R. P. Abbott

December 15, 2005

This work was performed under the auspices of the U.S. Department of Energy by University of California, Lawrence Livermore National Laboratory under Contract W-7405-Eng-48.

Ion Deflection for Final Optics in Laser Inertial Fusion Power Plants

by

Ryan P. Abbott

B.S. (University of California) 2002

A project submitted in partial satisfaction of the

requirements for the degree of

Master of Science

in

Engineering: Nuclear Engineering

in the

GRADUATE DIVISION

of the

UNIVERSITY OF CALIFORNIA AT BERKELEY

Committee in charge:

Professor Per F. Peterson, Chair
Professor Brian D. Wirth
Jeffery F. Latkowski, Ph.D.

December, 2005

The report of Ryan P. Abbott is approved:

_____

Chair Date

_____

Date

_____

Date

University of California, Berkeley

2005

ABSTRACT

Left unprotected, both transmissive and reflective final optics in a laser-driven inertial fusion power plant would quickly fail from melting, pulsed thermal stress, or degradation of optical properties as a result of ion implantation. One potential option for mitigating this threat is to magnetically deflect the ions such that they are directed to a robust energy dump. In this paper we detail integrated studies that have been carried out to assess the viability of this approach for protecting final optics.

I. INTRODUCTION

Inertial confinement fusion (ICF) is a process that can be initiated by forcing small targets containing deuterium and tritium (DT) to states of high density and temperature using heavy-ion, pulsed power, or laser drivers. As the fusion reactions consume the DT fuel, energetic photons, neutrons, and ions stream away in all directions. With powerful enough drivers coupled to properly designed & fabricated targets, the released energy can be significantly more than is needed to initiate the fusion "burn". This has led some to propose designs for power plants based on the harnessing of inertial fusion energy (IFE) [1, 2, 3]. Fig. 1 shows depictions of the heavy-ion driven HYLIFE-II chamber and the z-pinch (pulsed power) driven Z-IFE chamber.

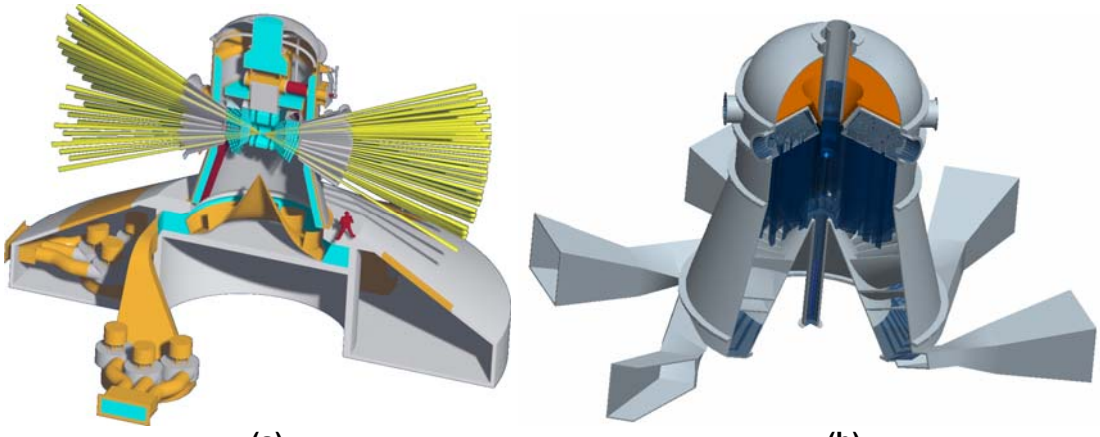

(a) (b)

Fig. 1 CAD Renders of two IFE reactor concepts. (a) The heavy-ion driven thick-liquid protected HYLIFE-II chamber and (b) the beamless Z-Pinch driven chamber.

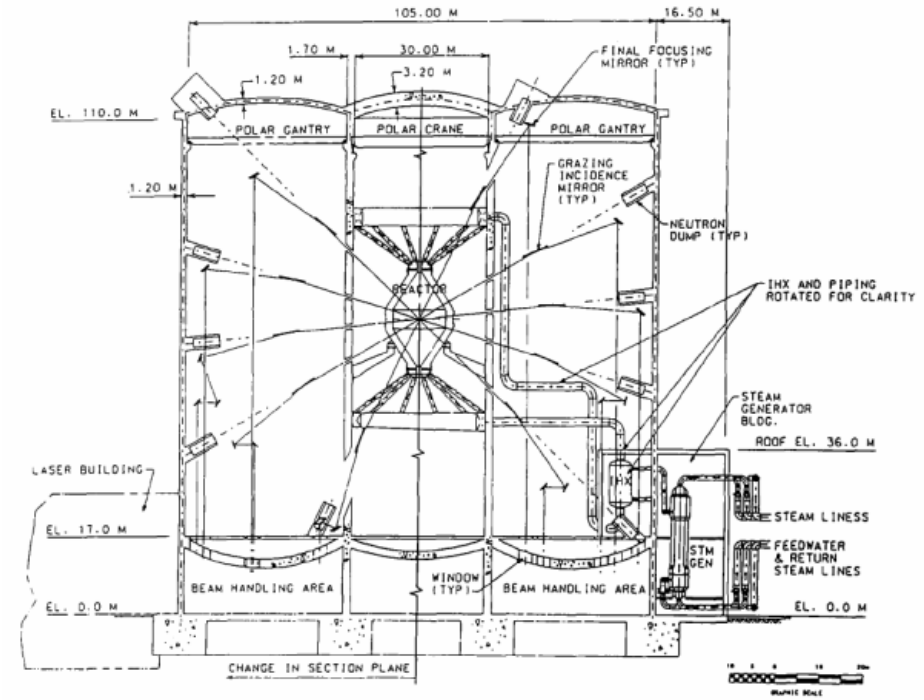

Fig. 2 A layout showing the SOMBRERO power plant's reactor situated in a 100 m diameter housing with lasers directed to chamber center by grazing incidence metal mirrors.

The SOMBRERO point design shown in Fig. 2 advocated a krypton fluoride (KrF) laser driver [4], while more recent progress in the development of the diode-pumped solid-state laser (DPSSL) under the high average power laser program (HAPL) has helped make it a viable option as well [5]. Both lasers could employ a grazing incidence metal mirror (GIMM) as the final optic, but the DPSSL also has the option of using a transmissive silica optic in the form of a Fresnel lens [6].

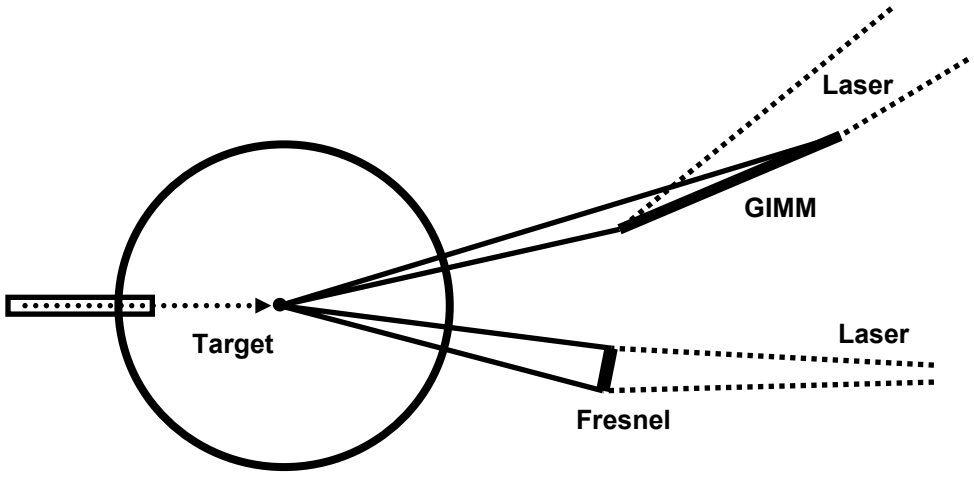

Fig. 3 A diagram showing the orientation reflective GIMM and transmissive Fresnel final optics would assume in a laser-driven IFE power plant.

Both transmissive and reflective final optics will face performance and survivability threats from the three types of energetic particles produced during DT fusion reactions: photons, neutrons, and ions. The SOMBRERO design addressed the threat from ions by calling for a xenon background gas in the target chamber at a number density of 1.8×10^{22} m^{-3}. At this density, the ions would slow in and heat the xenon which would then re-radiate this energy to the first wall and final optics in the form of x-rays over a considerably longer time period. The benefit of this would be to reduce the temperature spikes and thermal stresses on these components to acceptable levels [7].

As the cryogenic targets need to be kept below the DT fuel's triple point temperature of 21 K so that a stable implosion to be achieved, target heating during injection and transit through the chamber was considered. The SOMBRERO report concluded that while the target would experience a convective heat flux from the xenon gas of 4.2×10^4 W/m^2, this would be dominated by the irradiative heating of 5.4×10^5 W/m^2 from exposure to the IR given off by the hot first wall at approximately 1758 K [8]. It was estimated that the target's polystyrene surface would reach 700 K by the time it got to the center of a 6.5 m radius chamber when injected at 150 m/s and this was identified as an area for further study.

Unfortunately, while more recent target design calculations have shown that the irradiative heating can be reduced by 96% via the addition of a reflective high-Z (currently gold and palladium) layer to the target outer surface, xenon condensing on the target during injection has been identified as a heating mechanism far superior to the convective model considered in the SOMBRERO report and is now viewed as the greatest thermal challenge facing the design of survivable targets. And while the robustness of capsules could be significantly improved by addition of an insulating foam layer, background xenon gas densities will still have to be reduced by a factor of ten to fifty from those called for in the SOMBRERO design [9]. Some have even advocated its elimination altogether. This constraint has had a significant impact on several aspects of the chamber design with one of the most critical being the survival of the final optics.

With a background xenon density of 1.6×10^{22} m^{-3} (0.5 torr at 300 K) a surface 26 m from chamber center could expect to see a ^{4}He ion fluence of 8.1×10^{14} m^{-2} per shot with an average energy of 220 keV from the standard 350 MJ HAPL direct drive target. If this density must be reduced fifty fold, the fluence increases to 1.9×10^{16} m^{-2} with an average energy of 4.3 MeV. Bubble and blister formation is well documented in aluminum irradiated at fluences as little as 5×10^{21} m^{-2} [11]. This corresponds to just over 7 days for a GIMM inclined at 85° in an IFE power plant running at a frequency of 5 Hz. Fig. 4 illustrates how 3.6 MeV ^{4}He ions (the most probable helium ion energy) penetrate a xenon gas at these two density conditions.

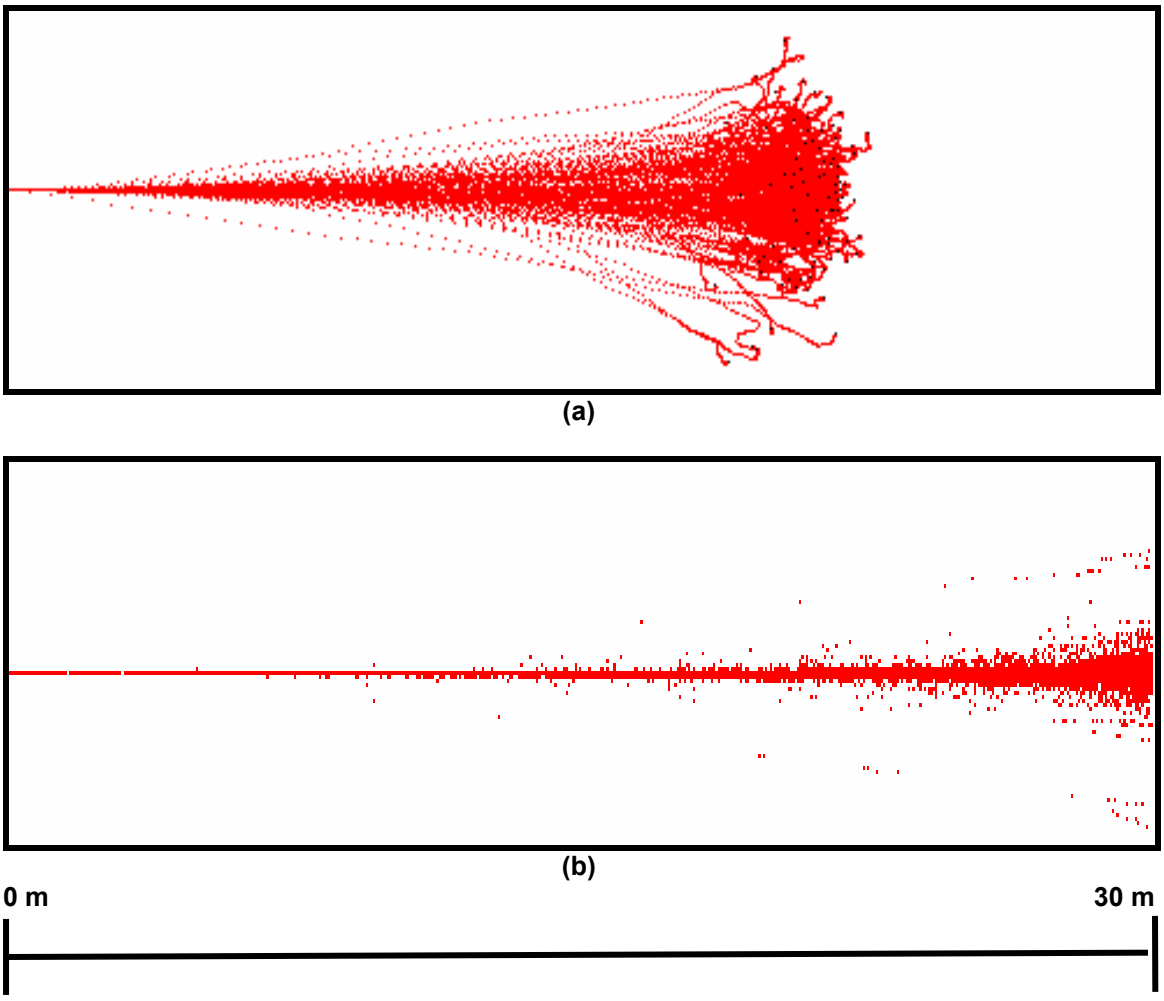

Fig. 4. SRIM plots showing the penetration of 3.6 MeV ^{4}He ions through xenon at densities of (a) 1.61×10^{22} and (b) 3.2×10^{20} m^{-3} (0.50 and 0.01 torr at 300 K).

Moreover, calculations modeling the ion deposition in a GIMM under these conditions indicate that the compressive stresses produced by ion heating could force its surface into plastic compression and pose a severe cracking threat. The relatively low thermal conductivity of SiO_2 leads to a bleaker story for a Fresnel. Similar calculations indicate that their surfaces will reach silica's melting temperature of 2100 K every shot.

One possibility for reducing or eliminating the threats to final optics from ion irradiation would be to magnetically deflect it into robust energy dumps such as the beam tube walls. Fig. 5 illustrates this concept showing a xenon filled target chamber and laser beam tube along with a magnetic field generated by a pair of electromagnetic coils. Also depicted are three possible resulting ion trajectories. The first shows the path of an ion stopped by the background gas. The second shows a deflected ion that still manages to reach the final optic and the third shows a successfully perturbed ion incident on the beam tube wall.

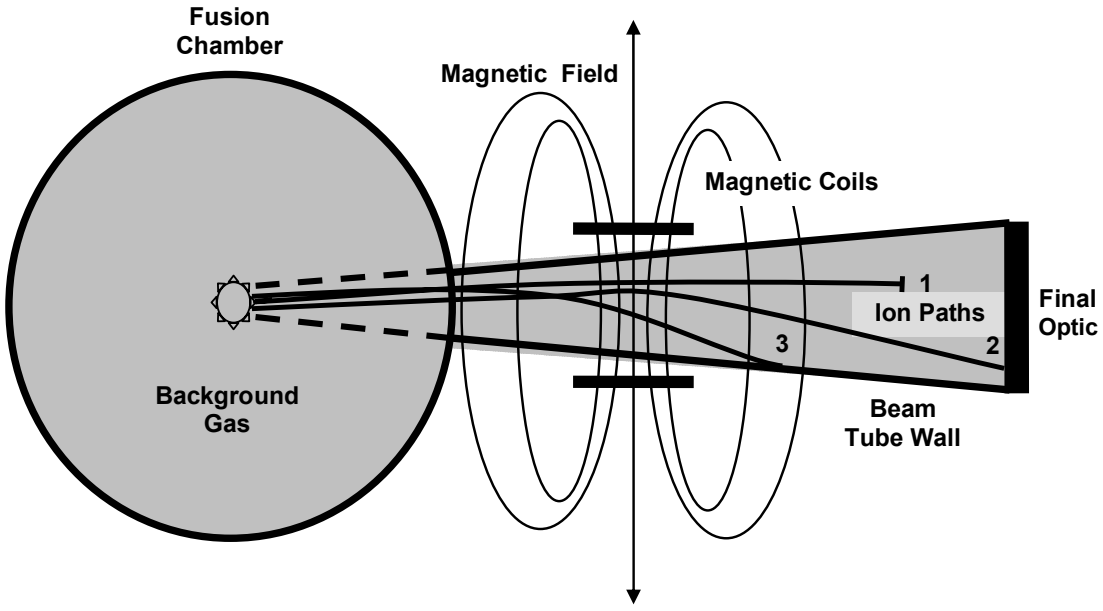

Fig. 5 A depiction of the ion mitigation concept showing three possible ion paths: (1) stopping in the background gas, (2) an optic intercepting path, and (3) a path showing an ion successfully deflected into the beam tube wall.

This paper details integrated calculations showing that a system like that shown in Fig. 5 can be used to protect each of the 60 (48 for a power plant using Fresnels) final optics in a laser IFE power plant. We demonstrate that modest fields which can be generated using normally conducting electromagnetic coils are sufficient to drastically reduce the ion fluence on the final optics. Estimates of how much power these systems will require along with their material costs are provided and show that this solution can be implemented with reasonable impact to the initial and operational costs of an IFE plant.

II. ION TRANSPORT PHYSICAL ASSUMPTIONS AND MODELING

II. A. The Deflector Code

A code called Deflector has been written that allows evaluation of the effectiveness of the magnetic deflection scheme depicted in Fig. 5. It can be setup to simulate what will happen for a variety possible final optic and chamber configurations, magnetic coil parameters, and background gas conditions. Essentially, it takes in user specified chamber geometry, magnetic field profile, background gas conditions, and ion spectra data and proceeds to determine the paths the ions will follow from their birth at chamber center to their ultimate positions either stopped in the background gas or impacting the beam tube wall or final optic. These paths are dependent on each ion's initial trajectory, how they loose kinetic energy, their charge state evolution, and their interaction with the coil generated magnetic field. A plot of output data for a typical Deflector simulation is shown in Fig. 6. In the sections that follow, we detail some key aspects of the Deflector code and how it determines the manner in which ions will stream from the target and be deflected from impacting final optics.

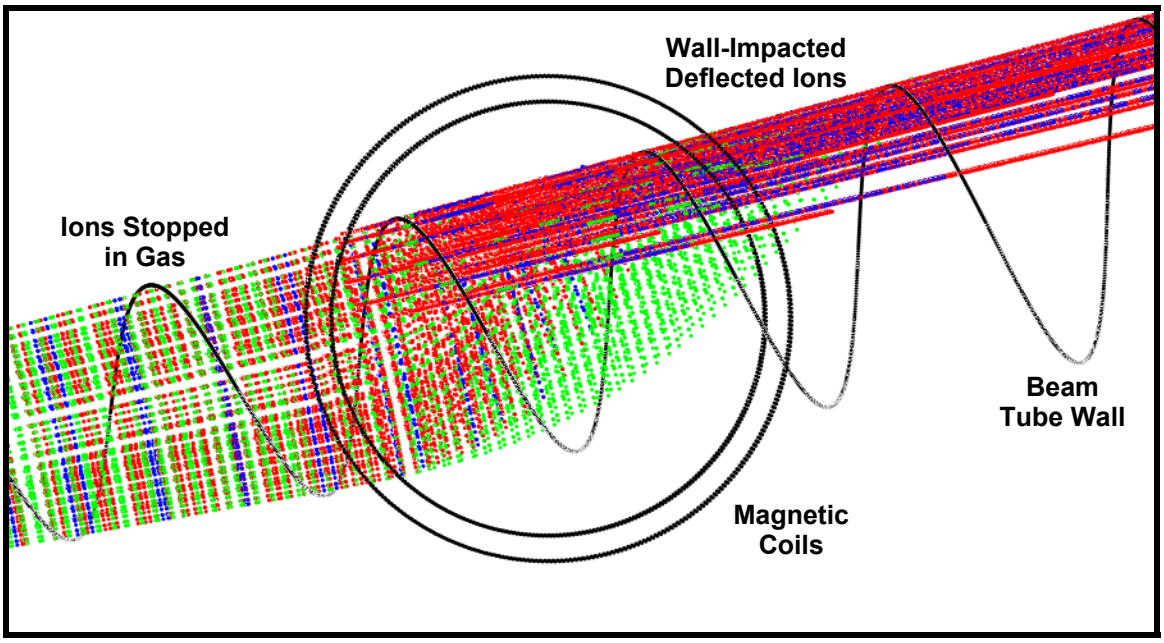

Fig. 6 A visualization of some components of Deflector's output data. Each colored point shows the stopping position of a simulation ion. Different colors represent the different species in the 350 MJ HAPL direct drive target: hydrogen (red), helium (blue), carbon (green), palladium (magenta), and gold (yellow).

II.B. Use of Simplified and Conservative Charge State and Stopping-Power Assumptions

For ions penetrating solid density thick targets, an examination of the charge exchange (ionization and recombination) reaction rates shows that the time scale over which the ions reach an equilibrium charge state is essentially instantaneous when compared to that for their stopping [12]. This allows treatment of the two processes to be decoupled by assuming an instantaneous stopping-power (an ion's loss of energy per unit length of penetration) based on an ionic equilibrium charge state that is a function of its instantaneous velocity.

However, in their transit through rarefied gas targets, such as the low density xenon fill gas that might be present in a laser IFE target chamber, ionization and recombination processes can occur on timescales comparable to that of the stopping processes. Therefore, a rigorous treatment of the ion-plasma interactions that determine the slowing and charge state evolution of swift ions traversing a low density ionized background gas has been a historically difficult task. The discrete reaction calculations

required are dependent on models to estimate charge exchange cross sections. These models have often been in gross error when compared to experiment, especially for plasma targets where the ion stripping is enhanced. Fortunately, resorting to such complicated and error prone calculations was not necessary when writing Deflector's ion transport algorithms.

Because our task is to deflect ions away from final optics with magnetic fields or have them stop in the background gas, any algorithm we choose that underestimates both the charge states ions will assume and the energy loss rates they will experience will be conservative. For a given calculation, we would predict less ion interaction with the magnetic fields (via $\mathbf{F} = q\mathbf{V}\times\mathbf{B}$) and less slowing in the background gas which would make it easier for ions to reach the final optics. In reality, the ions emerge from the target highly stripped. Since stopping is enhanced at charge states higher than equilibrium, it is conservative to assume that the ions will always be in an equilibrium charge state. Further, it is conservative to assume that the ions transport through a cold (non-ionized) background gas as stopping processes are enhanced by plasmas [13]. These approximations ensure that the ion deflection scheme would actually perform better than Deflector would predict.

To determine the slowing characteristics for each simulation ion at each point in time, Deflector interpolates data contained in stopping-power tables generated with SRIM. These calculations are independent of Deflector's calculation of an equilibrium charge state value using Eq. 1, an expression proposed by Bohr, Betz, Brown, and Moak [14] where Q_E is the equilibrium charge state, Z the ion's atomic number, v its velocity, α the fine structure constant, and c the speed of light.

$$Q_E = Z\cdot\left(1 - e^{\frac{-v}{Z^{\frac{2}{3}}\cdot\alpha\cdot c}}\right) \qquad \textbf{Eq. 1}$$

II.C. Magnetic field calculations

The magnetic field profiles used by Deflector were generated via direct integration of the Biot-Savart equation [15] for coil pairs in Helmholtz and non-Helmholtz configurations. Fig. 7 shows the results of such a calculation. At every point along a simulation ion's path, the magnetic force it will experience due to this field is determined. Field profiles can be scaled in both dimension and strength and their position modified in order to find an optimal configuration.

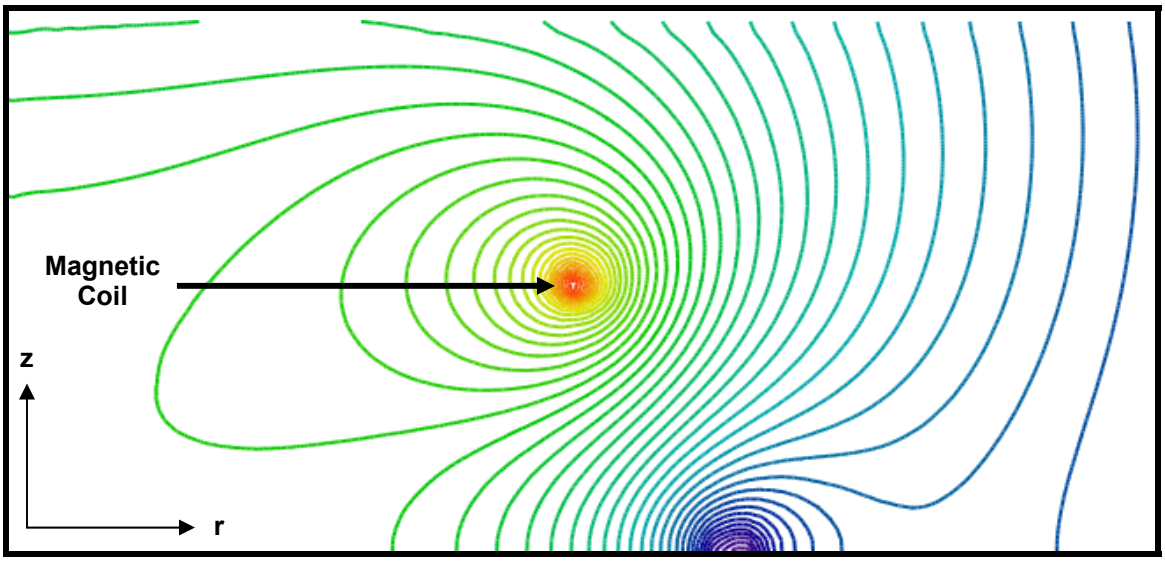

Fig. 7 A visualization of the axially symmetric magnetic field profile generated by a current carrying coil pair that will be used to deflect ions from final optics. The bottom of the plot lies on the mid-plane of the two coils and the left border sits on the axis of rotational symmetry for the system.

II.C. Plasma E and B fields

Deflector uses an independent particle model and transports an appropriate simulation ion along a variable number of initial trajectories for each energy group of the user supplied target ion spectra. In reality, all the ions will be traversing the chamber at the same time and this calculation methodology neglects the possibility of their being significant plasma generated electric and magnetic fields to counter the external magnetic field imposed by the coil pair. Three-dimensional simulations were run with the particle-in-cell code LSP and showed no external magnetic field distortions with plasma fields on

the order of 10^{-6} T . This is due primarily to the relatively low ion current densities that would be seen at the deflection magnet positions (≈ 12 m from chamber center). (D. Rose, personal communications, August 2005).

II.D. Ion charge state distributions and neutral fractions

While it may be true that assuming an equilibrium charge state for a simulation ion is conservative in that the actual average charge state for the billions of physical ions it represents will certainly be greater, this treatment ignores the fact that those ions will display a charge state distribution about that mean. If the coefficient of variation for those distributions is large, a significant fraction of the physical ions could at any given time be less affected by an external magnetic field than the assumption of a single equilibrium charge state for their simulation ion would have us believe.

For light ions ($^{1,\ 2,\ 3}$H, $^{3,\ 4}$He) only a few possible ionization states exist with neutrality just a couple of electron captures away from any attainable equilibrium or maximum ionization state. This makes the possibility of a significant neutral fraction at least qualitatively likely when compared to that for heavier ions expected to experience high equilibrium charge states. To estimate the likelihood of this occurring, the code CHARGE (a component of LISE++ [16]) was used to determine the neutral fraction distributions and ionization cross sections for both hydrogen and helium across their fusion ion energy spectrum after passing through xenon target thicknesses of ≈ 7×10^{-4} kg/m^2 (10 m of xenon at 0.01 torr and 300 K). Fig. 8 shows the ^{2}H and ^{4}He spectra for the 350 MJ direct-drive HAPL target and Fig. 9 gives the results of the neutral fraction calculations.

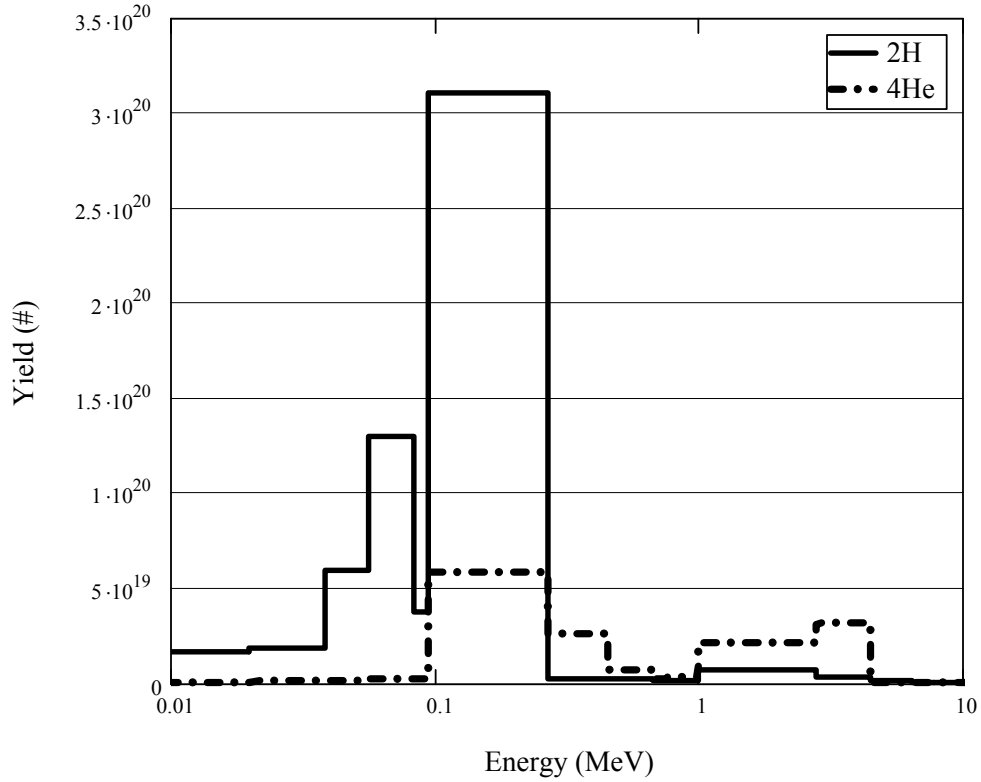

Fig. 8 ^{2}H and ^{4}He spectra from the 350 MJ direct-drive HAPL target.

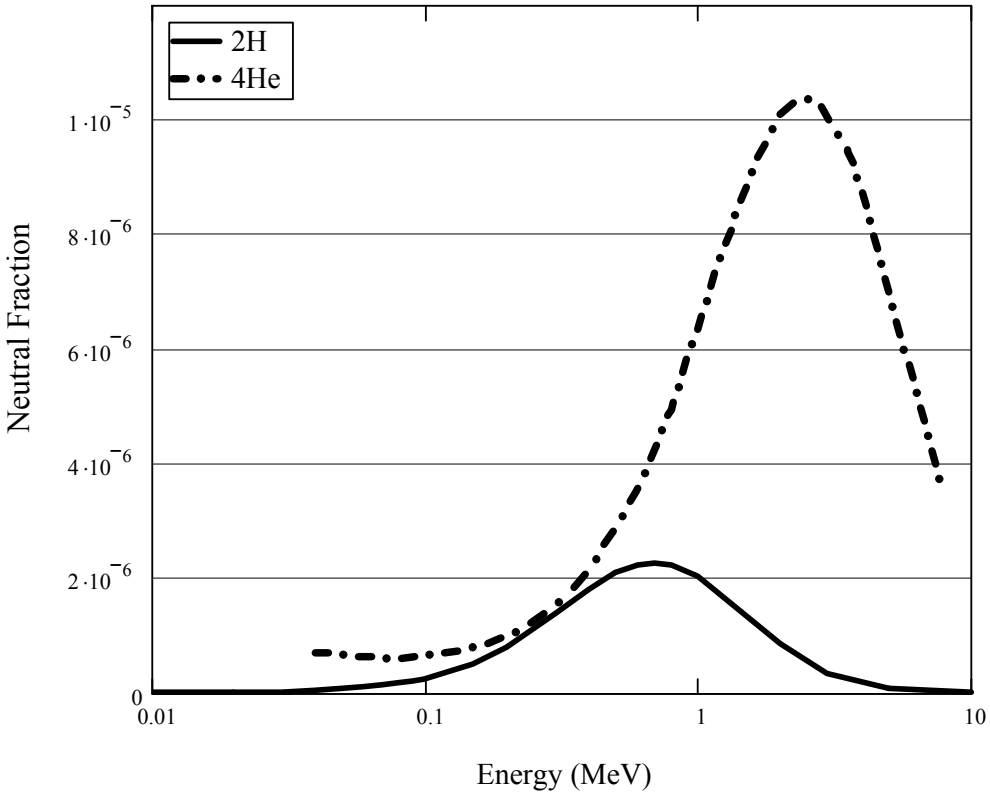

Fig. 9 ^{2}H and ^{4}He neutral fraction distributions obtained using the code CHARGE.

Even the small numbers from Fig. 9 drastically overestimate the threat of neutrals, though. An examination of the ionization cross sections shows that the mean free path for such reactions for a 1 MeV ^{4}He ion, for example, is only ≈ 7 μm in xenon at 10 mtorr and 300 K. This means that while at any given time one in 10^5 of these ions may be neutral, that will not be the case over any significant propagation distance and all light ions will be deflected by the magnetic field as if they were constantly at the equilibrium charge value.

Examination of Figs. 10 and 11 reveals that expected equilibrium ionization states for the heavy palladium and gold ions will be between 4^+ and 8^+. Charge state distribution widths show great regularity and can be estimated by the Eq. 2 where Z is the ion's atomic number and d_1 and w have been determined to be 0.32 and 0.45 for ions passing through argon and will be assumed the same for xenon here [17]. Fig. 12 shows the expected distribution widths for these ion species. A simple subtraction of half these values from the expected equilibrium charge states of Pd and Au shows there is little risk of a significant neutral fraction. However, carbon ions ($^{12,\ 13}$C , the last target output species) will experience equilibrium charge states closer to neutrality.

$$d = d_1 \cdot Z^w \qquad \textbf{Eq. 2}$$

Fig. 12 is the spectrum plot for carbon and Fig. 13 illustrates how these abundant medium mass ions will exhibit equilibrium charge states much closer to neutrality than palladium or gold. Still, Fig. 13 shows that carbon's charge state distribution will not cross the neutral threshold until energies below those the vast majority of carbons will be at. And, once again, even if a significant neutral fraction were to be expected, the ionization cross section for a 1 MeV carbon shows that any individual ion would not remain neutral for more than ≈ 0.4 cm and the assumption taken by Deflector that all ions are constantly at the equilibrium value is again justified.

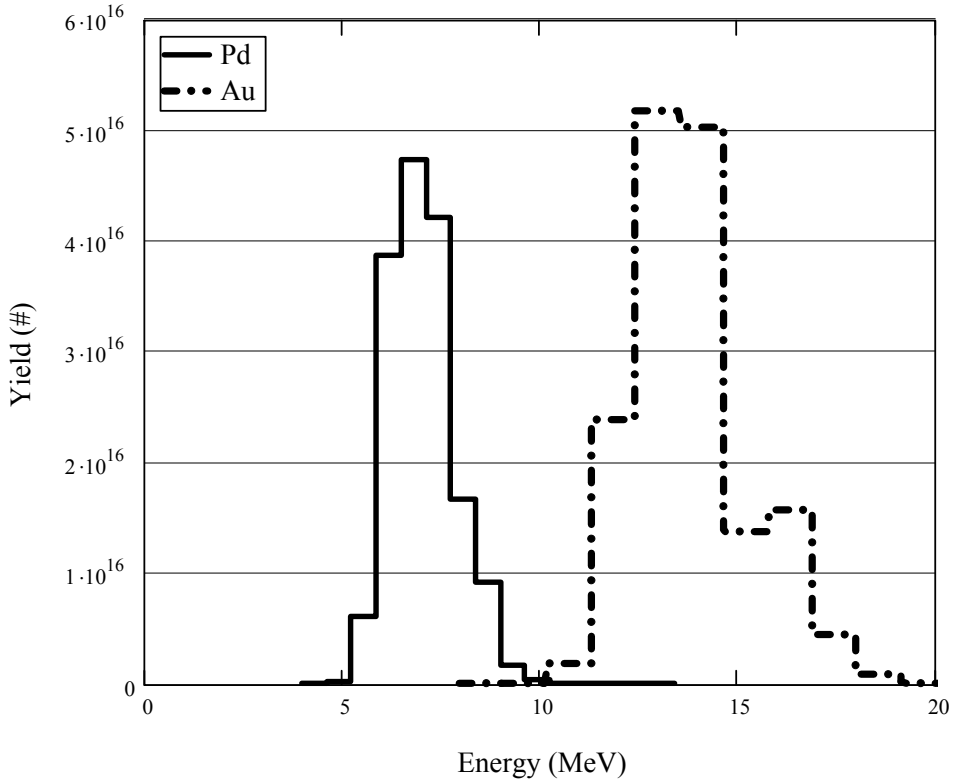

Fig. 10 Pd and Au ion spectra from the 350 MJ direct-drive HAPL target.

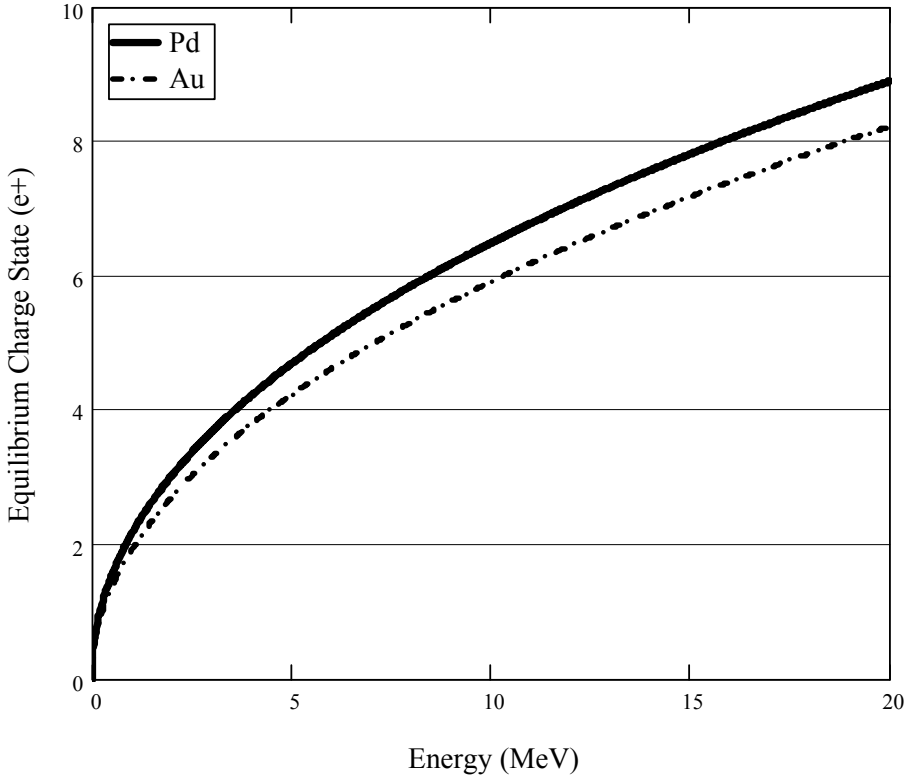

Fig. 11 Equilibrium charge curves for Pd and Au.

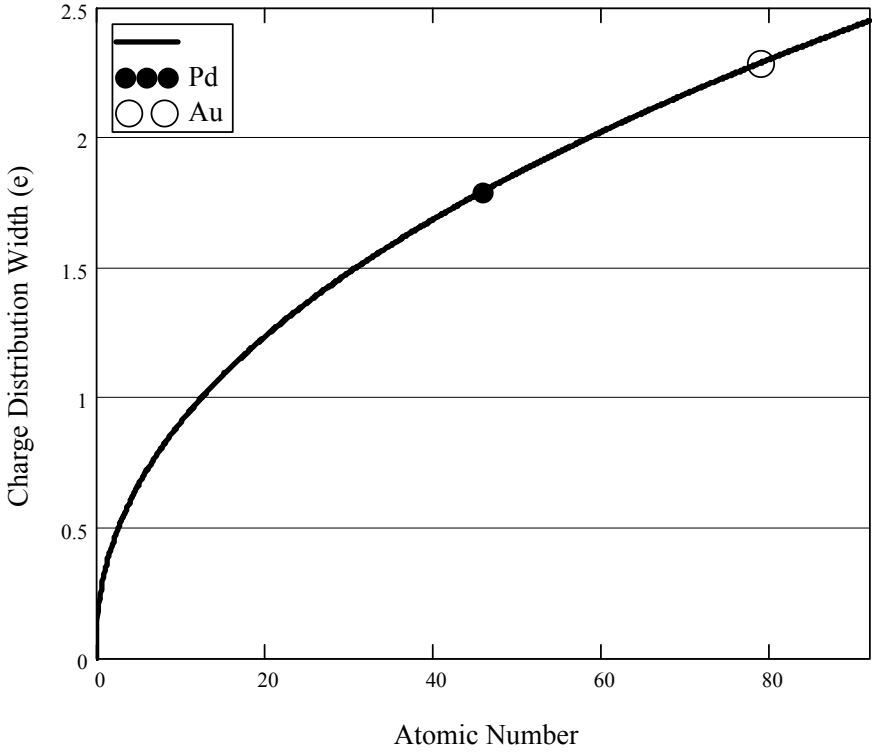

Fig. 11 Charge state distribution widths as predicted by Eq. 2 for all elements with those for $_{46}$Pd and $_{79}$Au.

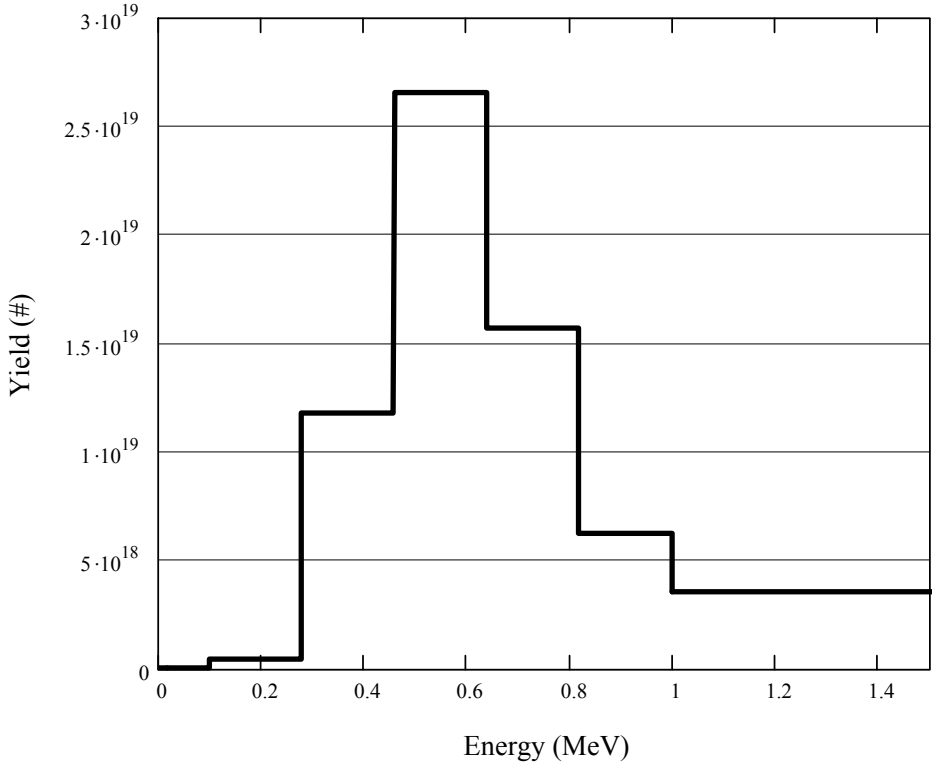

Fig. 12 The ^{12}C ion spectrum from the 350 MJ direct-drive HAPL target.

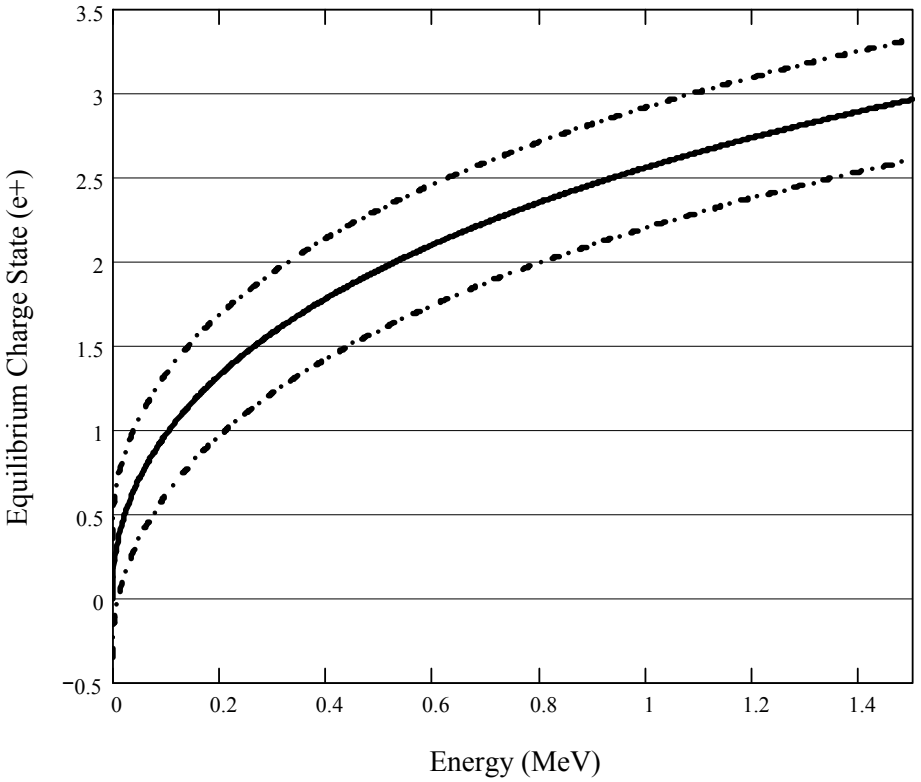

Fig. 13 Equilibrium charge curve for $_6$C. The dotted curves show the charge state distribution about this equilibrium as predicted by Eq. 2.

III. ION TRANSPORT RESULTS

Transient temperature analyses for the baseline HAPL program assumption of a tungsten armored first wall at the lowered xenon background gas pressures show that the target chamber will need a radius greater than 10 m to avoid significant damage [18]. For this work we have assumed the coil pairs will be placed 13 m from chamber center and the final optics have been granted a nominal target standoff distance of 26 m. Therefore, the deflected ions have approximately 13 m of beam tube wall over which they can impact before becoming a direct threat. The beam tube wall is modeled (as shown in Fig. 5 and Fig. 6) as right circular cone expanding from the target ignition point with some given divergence half-angle. The final optic position is treated simply as a critical plane normal to rays coming from chamber center, though, in reality they will be inclined quite a bit (85°) in the case of GIMMs. Our treatment of their placement when determining if ions reach them is conservative in this respect.

While both types of optics will be located at the same distance from chamber center, their orientation characteristics, the number of optics required, the type of driver used and uncertainty about laser fluence limits results in varying beam tube half-angles. Moreover, depending upon what type of laser is used (KrF or DPSSL) more or less drive energy is needed. Table 1 summarizes the base-cases for which coil sizes were determined to result in configurations providing a reduction in ion fluence at the final optics by a factor of approximately 10^4; a value providing ~ 3 yr before the onset of blistering in Fresnels expected to occur at a fluence of ~ 10^{21} $_4$He/m^2 [23]. The details of two of the configurations are outlined below and Table 2 gives the pertinent simulation details and results for all configurations.

CASE	OPTIC TYPE	DRIVER TYPE	LASER FLUENCE LIMIT (J/m^2)	BEAM TUBE HALF-ANGLE
1	GIMM	KrF (2.46 MJ)	5×10^4 ($\perp$ to beam)	1.13°
2	GIMM	DPSSL (3.02 MJ)	5×10^4 ($\perp$ to beam)	1.25°
3	Fresnel	DPSSL	2×10^4	2.21°
4	Fresnel	DPSSL	4×10^4	1.56°
5	Fresnel	DPSSL	6×10^4	1.27°

Table 1. Evaluated base-cases for ion deflection concept. A set of configurations were selected covering possible use of both driver technologies (KrF and DPSSL), both final optic options (GIMM and Fresnel), and various laser fluence limits.

III.A. Case 1

This case assumes a GIMM final optic with its center located 26m from chamber center. To accommodate a required KrF drive energy of 2.46 MJ across 60 beam-lines and a GIMM laser fluence limit of 5×10^4 J/m^2 necessitates a beam-tube half-angle of 1.13° (assuming right circular conical tubes). The target yield is 365 MJ [19]. Supplying Deflector with these parameters along with a center-of-coil-pair (COCP) magnetic field strength of 7.5×10^{-2} T and a profile consistent with a Helmholtz configuration of 1.0 m diameter coils yields the results in Fig. 14 and a reduction in ion number-fluence (#/m^2) to the final optics by a factor of 4.8×10^4 and energy fluence (J/m^2) by a factor of 1.4×10^3 (energetic particles are more difficult to deflect).

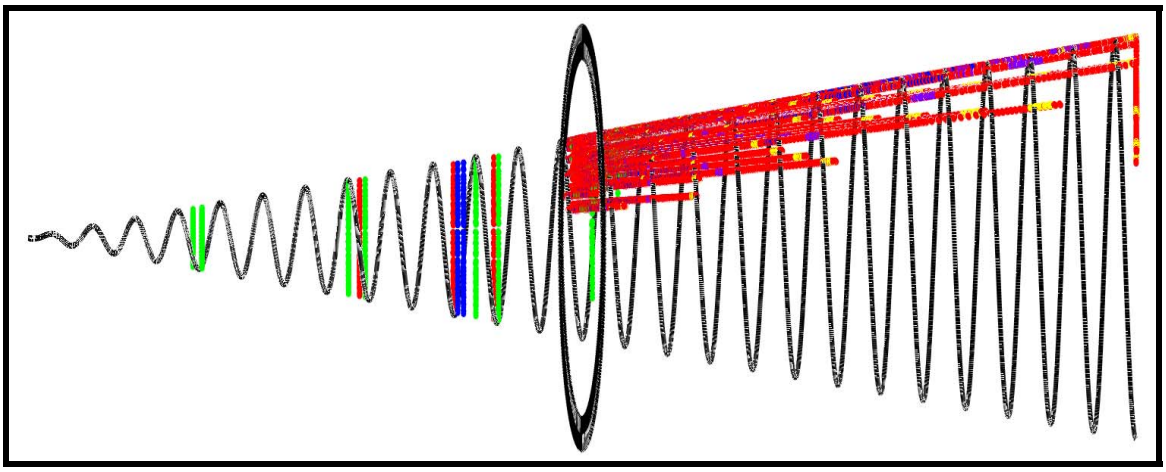

Fig. 14. A visualization (not to scale) of Deflector output date for Case 1. As can be seen, very few ions reach the final optic with most being deflected into the beam tube wall.

III.B. Case 3

This case assumes a Fresnel final optic also positioned 26m from the target. To accommodate a required DPSSL drive energy of 3.02 MJ across 48 final optics and a laser fluence limit of 2×10^4 J/m^2 necessitates a beam-tube half-angle of 2.21°. The target yield is 383 MJ. These parameters along with a field strength of 7.5×10^{-2} T from a 1.8 m diameter coil pair result in a reduction in number-fluence by a factor of 2.0×10^5 and energy fluence by a factor of 6.3×10^2.

CASE	COIL DIA. (m)	COCP FIELD STRENGTH (T)	AT COIL FIELD STRENGTH (T)	# FLUENCE REDUCTION (N_0/N)	E FLUENCE REDUCTION (E_0/E)
1	1.0	7.5×10^{-2}	1.8×10^{-1}	4.8×10^4	1.4×10^3
2	1.0	7.5×10^{-2}	1.8×10^{-1}	1.4×10^4	4.3×10^2
3	1.8	7.5×10^{-2}	2.3×10^{-1}	2.0×10^4	6.3×10^2
4	1.3	7.5×10^{-2}	2.0×10^{-1}	2.5×10^4	7.7×10^2
5	1.0	7.5×10^{-2}	1.8×10^{-1}	1.2×10^4	3.8×10^2

Table 2. A Summary of ion fluence reduction results for Deflector analyzed base-case configurations.

V. THE SPUTTERING THREAT

Energetic deflected ions impacting beam tube walls and generating potentially life-limiting final optic contamination was a distinct possibility warranting further investigation. To quantify this threat, ion impact angles, positions, and energies were tabulated with Deflector and combined with SRIM-generated "sputtering yield" tables to estimate sputtering product characteristics and determine an upper bound on how much might reach the final optics. Fig. 15 shows impact angle distributions for Case 5 of Table 2.

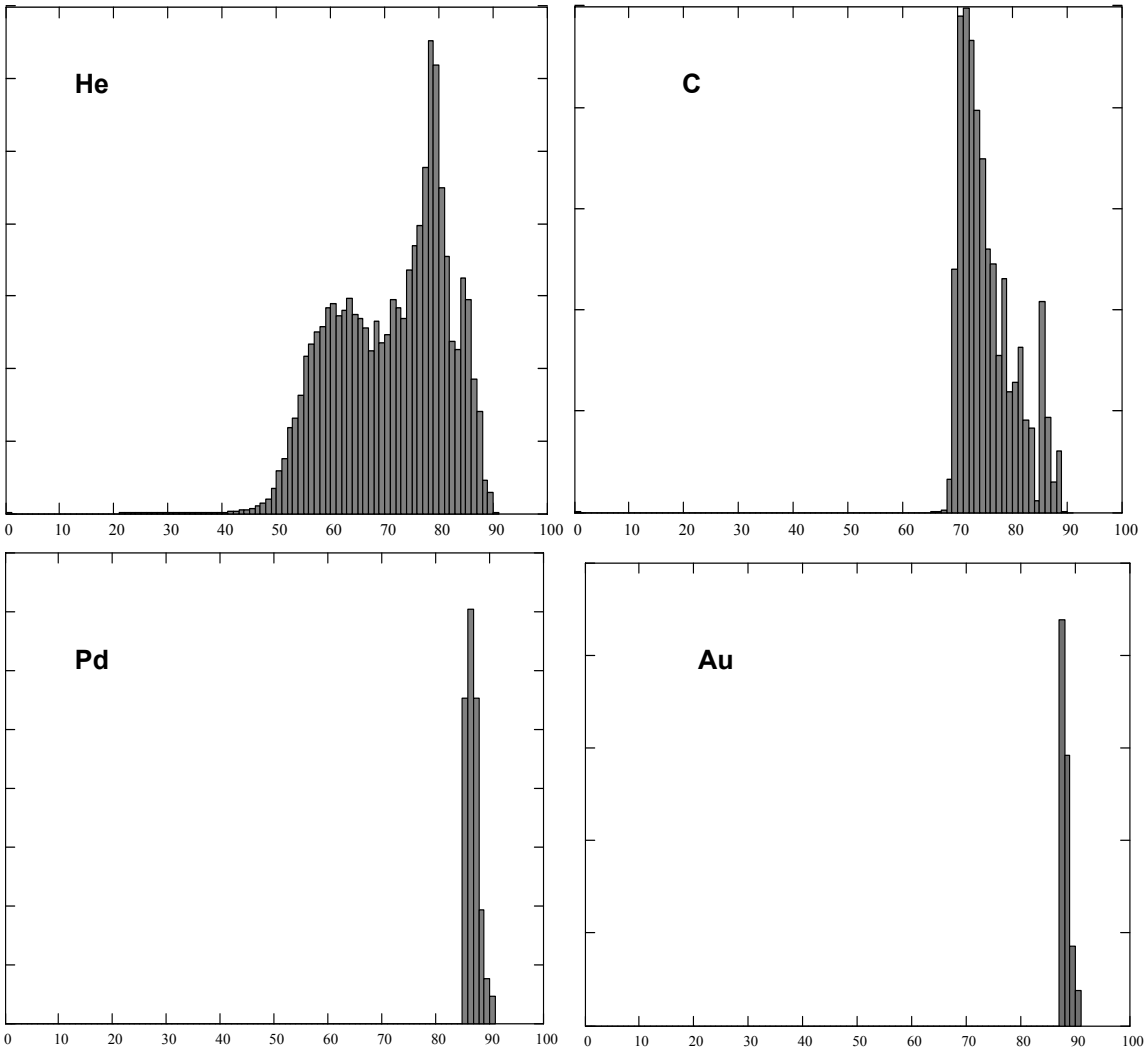

Fig. 15. Impact angle (0° is normal incidence) distributions for He, C, Pd and Au ions deflected into the beam-tube walls.

For each ion species SRIM was used to generate tables characterizing the sputtering products expected from impacts with the tungsten beam-tube wall material as a function of impact angle and energy. These tables were combined with Deflector results detailing the location, frequency, and angle distribution of ion impacts to determine an upper limit on the amount of sputtering products that could potentially reach the final optics. Table 3 shows an example of "sputtering yield" tables for gold.

	84°	85°	86°	87°	88°	89°
10 MeV	27	33	39	47	63	51
12 MeV	25	28	35	43	55	50
14 MeV	21	27	35	43	57	51
16 MeV	20	24	34	43	52	53
18 MeV	20	25	26	39	50	55
20 MeV	17	23	27	40	50	60

(a)

	84°	85°	86°	87°	88°	89°
10 MeV	3.2	3.1	3.4	3.6	2.3	3.4
12 MeV	3.5	4.4	3.7	2.8	4.9	3.1
14 MeV	2.5	4.3	2.6	3.4	2.7	4.8
16 MeV	2.5	4.8	3.0	2.3	4.0	4.2
18 MeV	2.8	3.3	1.7	5.7	3.2	2.8
20 MeV	3.5	3.7	2.0	3.3	3.8	2.6

(b)

Table 3. **SRIM generated "sputtering yield" tables for gold ions impacting a tungsten target at various IFE relevant angles and energies. (a) gives the average number of sputtered W atoms per gold impact ion at the given combination of impact energy and angle. (b) gives the average energy of those sputtered W atoms in keV.**

Table 4 gives the results of these calculations showing that only the gold ions produce any significant amount sputtering products that reach the final optics. This is primarily due to the fact that the sputtered tungsten atoms have kinetic energies of at most a few keV which gives them ranges of less than 1 m in the 3.2×10^{20} m^{-3} xenon background gas number density. It is unclear whether this estimate of the sputtering threat is significant or benign.

THREAT ION SPECIES	YIELD TO OPTIC (#/shot)
H	<< Au
He	<< Au
C	<< Au
Pd	<< Au
Au	2.9×10^{12}
Total	2.9×10^{12}

Table 4. **Estimates of the sputtering threat to final optics from magnetically deflected target output ions. Only gold ions had the energetics, impact angle and location characteristics to reveal a sputtering product yield of any significance for the final optics.**

V. SYSTEM POWER REQUIREMENTS AND MATERIAL COSTS

The power requirements for a full system of 48 or 60 coil pairs to protect Fresnel or GIMM final optics, respectively, can be estimated fairly easily using Eq. 3 where P is power (W), ρ the conductor resistivity (1.7×10^{-8} Ω×m for Cu), λ the conductor to coil cross-sectional area ratio (≈ 0.8), μ_0 the permeability of vacuum ($4\pi \times 10^{-7}$ N/A^2), and the other parameters are as defined in Fig. 16 with the COCP field strength B_z in Tesla and the geometric factors (R_1, L_1, etc.) in meters [20]. Table 5 gives the estimated power requirements for each deflection case detailed in Table 2 along with required coil cross sections based on the current density limit of 5×10^6 A/m^2 for copper [21].

$$P = \left(\frac{B_z}{\mu_0 \cdot G}\right)^2 \cdot \frac{R_1 \cdot \rho}{\lambda} \qquad \textbf{Eq. 3}$$

$$G = \sqrt{\frac{1}{2 \cdot \pi \cdot \left(\alpha^2 - 1\right) \cdot \left(\beta_2 - \beta_1\right)}} \cdot \left[\left(\beta_2\right) \cdot \ln\left(\frac{\alpha + \sqrt{\alpha^2 + \beta_2^2}}{1 + \sqrt{1 + \beta_2^2}} \right| \ldots \right.$$
$$\left. + \left(-\beta_1\right) \cdot \ln\left(\frac{\alpha + \sqrt{\alpha^2 + \beta_1^2}}{1 + \sqrt{1 + \beta_1^2}} \right| \right]$$

$$\alpha = \frac{R_2}{R_1} \qquad \beta_1 = \frac{L_1}{2 \cdot R_1} \qquad \beta_2 = \frac{L_2}{2 \cdot R_1}$$

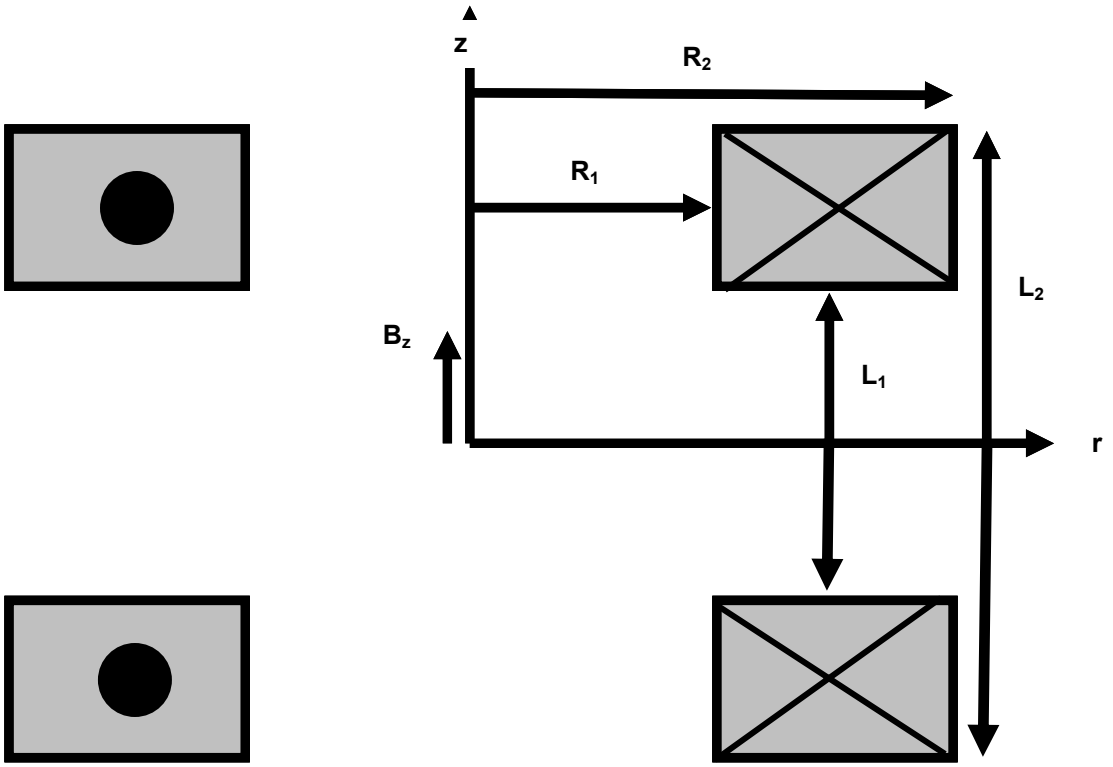

Fig. 16. A schematic of a field coil pair showing relevant parameters for determining its power requirements depending on the COCP field strength B_z.

CASE	CROSS SECTION (cm)	# OF COIL PAIRS	POWER / COIL (kW)	SYSTEM POWER (MW)
1, 2	L 8.9 × W 8.9	60	38	2.3×10^6
3	L 11.9 × W 11.9	48	116	5.6×10^6
4	L 10.1 × W 10.1	48	63	3.0×10^6
5	L 8.9 × W 8.9	48	38	1.8×10^6

Table 5. Power requirement estimates for ion deflection systems to protect all final optics in a power plant

If a cost of electricity (COE) of 5 ¢/kW-hr is assumed, the most power hungry system of deflection coils above (Case 3) would have an operational cost of at least 2.4 M$ / year. The costs for the raw coil materials (mostly copper) would be reasonable as well. At 10 $/kg, 48 1.8 m diameter coil pairs with 1.4×10^{-2} m^2 cross sections would cost roughly 680 k$. Obviously mounting hardware, installation, and extra neutron shielding requirements would raise this figure, but not by the orders of magnitude that

would be required for the initial cost to even compete with the power requirement costs, let alone the final COE for generated power.

VI. FURTHER WORK

Though we believe all the major feasibility issues of a magnetic deflection system to protect final optics have been addressed in the current body of research, there are several areas where further investigation would be valuable in increasing confidence such systems would in fact work. One potentially critical area where further efforts need to be focused is that of neutron shielding. The resistivity of copper has been observed to increase under fast neutron fluences [22] which would lead to decreased magnetic deflection effectiveness as less current would flow through the coils and weaker field strengths would be generated.

Beam tube heating and long term breakdown from deflected ion irradiation is also an area of concern. The coupling of Deflector results to a transient heat transfer code capable of treating penetrating radiation would show if there are any issues with excessive thermal loading on the beam tube walls in regions where the magnetic fields concentrate a large number of threat ions (just past the coil region in Fig. 14, for example). Ion irradiations of tungsten on accelerators with the threat ion species to IFE relevant fluences based on Deflector results would be useful in characterizing a beam tube's medium and long term response to the impact of deflected ions.

While the base-cases selected for analysis in this research reduce the ion threat substantially, it is likely that more optimized coil positions, magnetic field profiles, and beam tube geometries will lead to an even greater reduction in the threat to final optics. Automating Deflector for the purposes of conducting variation studies on these and other parameters may reveal more economic and effective ion deflection system configurations.

VII. SUMMARY AND CONCLUSIONS

Calculations have shown that excessive heating due to xenon condensation on targets during injection requires pressures of this protective background gas to be substantially lower than was previously assumed. Under these conditions, target output ions have been shown to be a significant life limiting hazard to final optics in a laser driven IFE power plant even when located several tens of meters from the ignition point.

This analysis of a simple magnetic deflection scheme shows that target generated ions can be successfully perturbed from trajectories that would otherwise lead to rapid or even single-shot failure of final optics. By using modest magnetic fields generated with normally conducing coil pairs, greater than 99.99 % of the ions that would otherwise threaten the final optics can be deflected into the laser beam tube walls.

The threat from sputtered atoms coming from ion impact sites on the beam tube walls has been quantified and bounded, though further analysis remains to determine if it is a credible secondary threat to the final optics. The power requirements for a full system of deflecting coils to protect all final optics would modest and the direct materials costs relatively inexpensive. The deflection coils may require substantial neutron shielding to protect the electrical properties of the conducting material but this issue has not been addressed.

VIII. ACKNOWLEDGEMENTS

The author would like to acknowledge the invaluable collaboration of Dr. Jeffery Latkowski on this research as well as critical input from Dr. Dave Rose.

This work was performed under the auspices of the U.S. Department of Energy by the University of California, Lawrence Livermore National Laboratory under contract No. W-7405-ENG-48.

VIII. References

[1] S. YU et al., "An Updated Point Design for Heavy Ion Fusion," *Fusion Sci. and Technol*. **44**, 266 (2003).

[2] W.R. Meier, "Osiris and SOMBRERO inertial fusion power plant designs summary, conclusions, and recommendations," *Fusion Eng. and Design* **25**, 145 (1994).

[3] G. E. Rochau, "Progress Toward Development of an IFE Power Plant Using Z-Pinch Technology," *Fusion Sci. and Technol.* **47**, 641 (2005).

[4] W.R. Meier et al., "OSIRIS and SOMBRERO inertial fusion power plant designs. Final report. Volume 2. Designs, assessments, and comparisons," Report #: WJSA-92-01 DOE/ER/54100-1-VOL-2 ,p. 3-11.

[5] C. Bibeau et al., "Full System Operations of Mercury: A Diode Pumped Solid-State Laser," *Fusion Science and Technology* **47**, 581 (2005).

[6] J.F. Latkowski et al., "Fused Silica Final Optics for Inertial Fusion Energy: Radiation Studies and System-Level Analysis," *Fusion sci. and Technol.* **43**, 540 (2003).

[7] W.R. Meier et al., "OSIRIS and SOMBRERO Inertial Confinement Fusion Power Plant Designs Volume2 - Designs, Assessments, and Comparisons," WJSA-92-01 DOE/ER/54100-1, p. 3-6, (1992).

[8] Ibid., p. 4-47.

[9] A.R. Raffray, "Target Thermo-Mechanical Modeling and Analysis," presented at the 7th High Average Power Laser Program Workshop, 2003, Retrieved December 7, 2005, from http://aries.ucsd.edu/HAPL/MEETINGS/0309-HAPL/raffraytarget.ppt#402,1,Slide 1

[11] S. Furan et. al., "Dynamic Behavior of Bubbles and Blisters in Aluminum During Helium Ion Irradiation in an Electron Microscope," *Journal of Nuc. Mat.*

[12] M. S. Armel, "Atomic Processes for Heavy Ion Inertial Fusion," Ph.D. dissertation, University of California, Berkeley, CA, USA, 2000, p. 93.

[13] E. Nardi and Z. Zinamon, "Charge State and Slowing of Fast Ions in Plasma," *Physical Review Letters*, **49**, 1251, (1982).

[14] M. D. Brown and C.D. Moak. *Phys. Rev. B*, **6**, (1972).

[15] Young and Freedman, University Physics with Modern Physics, 11th edition, Addison Wesley, San Francisco, 2004, p. 1066.

[16] "Simulation of Fragment Separators," Retrieved December 8, 2005, from http://groups.nscl.msu.edu/lise/lise.html

[17] H. D. Betz, "Charge States and Charge-Changing Cross Sections of Fast Heavy Ions Penetrating Through Gaseous and Solid Media," *Reviews of Modern Physics*, **44**, 465, (1972).

[18] A.R. Raffray, "Blanket Design for Large Chambers," presented at the 13th High Average Power Laser Program Workshop, 2005, Retrieved December 7, 2005, from http://aries.ucsd.edu/HAPL/MEETINGS/0511-HAPL/Tuesday/15.0Raffray.ppt

[19] L.J. Perkins, "HAPL Reactor Targets: Baseline Specifications and Future Options," presented at the 13th High Average Power Laser Program Workshop, 2005, Retrieved December 7, 2005, from (http://aries.ucsd.edu/HAPL/MEETINGS/0511-HAPL/Tuesday/05.0Perkins.ppt).

[20] E. Dennison, "Axial Field of a Real Helmholtz Coil Pair," Retrieved December 8, 2005, from http://www.netdenizen.com/emagnet/helmholtz/realhelmholtz.htm

[21] "Microscopic View of Copper Wire," Retrieved December 8, 2005, from http://hyperphysics.phy-astr.gsu.edu/hbase/electric/ohmmic.html

[22] Y. Iwasa, Case Studies in Superconducting Magnets, Plenum Press, New York (1994).

[23] S.B. Gilliam et al., "Retention and Surface Blistering of Helium Irradiated Tungsten as a First Wall Material," *Journal of Nuclear Materials*, **347**, 289, (2005).